Journal of Biomolecular NMR (2006) 36:111–122
DOI 10.1007/s10858-006-9068-z

Article

Mapping protein–protein interaction by $^{13}C'$-detected heteronuclear NMR spectroscopy

Ivano Bertini[a,b,*], Isabella C. Felli[a,b], Leonardo Gonnelli[b], Roberta Pierattelli[a,b], Zinovia Spyranti[c] & Georgios A. Spyroulias[c]

[a]*Department of Chemistry, University of Florence, 50019 Sesto Fiorentino, Italy;* [b]*Magnetic Resonance Center (CERM), University of Florence, Via Luigi Sacconi 6, 50019 Sesto Fiorentino, Italy;* [c]*Department of Pharmacy, University of Patras, 26504 Patras, Greece*

Received 3 March 2006; Accepted 19 July 2006

Key words: ^{13}C-NMR, chemical shift perturbation, copper chaperones, metal-mediated interaction, proteins complex, protonless NMR

Abstract

The copper-mediated protein–protein interaction between yeast Atx1 and Ccc2 has been examined by *protonless* heteronuclear NMR and compared with the already available ^{1}H–^{15}N HSQC information. The observed chemical shift variations are analyzed with respect to the actual solution structure, available through intermolecular NOEs. The advantage of using the CON-IPAP spectrum with respect to the ^{1}H–^{15}N HSQC resides in the increased number of signals observed, including those of prolines. CBCACO-IPAP experiments allow us to focus on the interaction region and on side-chain carbonyls, while a newly designed CEN-IPAP experiment on side-chains of lysines. An attempt is made to rationalize the chemical shift variations on the basis of the structural data involving the interface between the proteins and the nearby regions. It is here proposed that *protonless* ^{13}C direct-detection NMR is a useful complement to ^{1}H based NMR spectroscopy for monitoring protein–protein and protein–ligand interactions.

Abbreviations: δ – chemical shift; IPAP – in-phase-anti-phase

Introduction

The mechanisms of molecular recognition and interaction of macromolecules can only be studied in detail through the elucidation of the three-dimensional structure of the formed complexes. However, it is often possible to map the intermolecular contacts by analyzing the chemical shift variations in simple 2D NMR spectra. This is generally achieved by monitoring the spectral changes in a ^{1}H–^{15}N correlation map (Zuiderweg, 2002). However, the exchangeable amide protons (H^N) are very sensitive to any variation in their chemical environment and the understanding of the effects that cause these chemical shifts is rather weak (Wishart and Case, 2001; Neal et al., 2003). Indeed, several factors, such as torsional contributions, hydrogen bonds, ring current effects, do concur to the chemical shift of a nucleus but our ability to reproduce such shifts from back calculations for H^N is actually one of the lowest (Wishart and Case, 2001; Neal et al., 2003). Back calculation of N and C' chemical shifts still represents a challenge, while the chemical shifts of C^α and C^β are somehow better understood (Sitkoff and Case, 1998; Schwarzinger et al., 2001; Wishart and Case, 2001; Sun et al., 2002; Oldfield, 2002;

*To whom correspondence should be addressed. E-mail: ivanobertini@cerm.unifi.it

Neal et al., 2003). As they depend on different contributions in a different way, chemical shift mapping using a combination of chemical shift variations of different types of nuclei may be useful to monitor protein–protein interactions.

Over the past few years we have been involved in studying copper trafficking. Copper, like other metal ions, needs the so-called metallochaperones in its transport pathways within the cytoplasm (O'Halloran and Culotta, 2000; Rosenzweig, 2001). In *Saccharomyces cerevisiae* the copper chaperone Atx1 delivers Cu(I) to the soluble copper domains of Ccc2, an ATPase located in the trans-Golgi network (Pufahl et al., 1997) which then transfers copper to a cuproenzyme. Solution structures of the native Cu(I)-bound and the reduced apo-forms of both yeast Atx1 and the first soluble domain of Ccc2 (Ccc2a hereafter) have been solved in our laboratory (Banci et al., 2001; Arnesano et al., 2001b). These structures share a classical βαββαβ 'ferredoxin-like' folding, with the secondary structure elements connected by loop regions. The copper-binding motifs MXCXXC are located in a solvent-exposed region encompassing the first loop and the beginning of the first α-helix. Copper is coordinated by the two cysteines and is able to expand its coordination sphere to three-coordination by binding an exogenous ligand. Copper exchange between Atx1 and Ccc2 occurs through copper binding to both proteins. The adduct is present at the extent of 70% at millimolar concentration of all species (Arnesano et al., 2001a) and it represents a neat example of metal-mediated protein–protein interaction. The structure of the adduct has been extensively studied in solution (Banci et al., 2006) and we are now interested in analyzing at the molecular level the details of complex formation that can be obtained from chemical shift changes. Starting from the available structural information of the adduct we assess here the use of *protonless* ^{13}C direct-detection NMR experiments for monitoring complex formation and protein–protein interactions.

Materials and methods

Sample preparation

^{13}C,^{15}N enriched Atx1 and unlabeled Ccc2a from *Saccharomyces cerevisiae* were expressed in *Escherichia coli* and purified following previously reported protocols (Huffman and O'Halloran, 2000; Arnesano et al., 2001b; Banci et al., 2001). ^{13}C,^{15}N enriched labeled Ccc2a was purchased from ProtEra s.r.l. (Sesto Fiorentino, Italy) and used without further purification. Copper(I) was added directly in the NMR tube under inert atmosphere (Coy Lab), by adding small aliquots of an acetonitrile solution of tetrakis(acetonitrile)copper(I) hexafluorophosphate as copper source. Apo-proteins were added directly in the NMR tube as well.

For all samples the protein concentration was about 0.8–1.0 mM, 100 mM KPi in 90% H_2O/10% D_2O at pH 7.0 in the presence of substoichiometric amount of dithiothreitol (DTT). The apo-Atx1 sample was 2.0 mM in protein, the other conditions being the same.

NMR experiments and data analysis

The ^{13}C direct-detection experiments reported were recorded at 14.1 T with a Bruker Avance 700 NMR spectrometer equipped with a triple-resonance probe optimized for ^{13}C sensitivity (Bertini et al., 2004). Experiments were acquired with relaxation delays between 1.5 and 1.6 s and acquisition times ranging from 58 to 72 ms. The spectral widths were between 40 and 50 ppm for C′, 50 ppm for N, 50–60 ppm for C^{α} and 100 ppm for C^{ali}. The ^{1}H carrier was placed at 3.5 or 7 ppm and the ^{15}N carrier was placed at 118 ppm, respectively; composite pulse decoupling was applied during acquisition and during some of the elements of the pulse sequence with RF field strengths of 1.6 kHz for ^{1}H (waltz-16) (Shaka et al., 1983) and 0.625 kHz for ^{15}N (garp-4) (Shaka et al., 1985). ^{13}C pulses were given at 176.75, 57.75 and 41.75 ppm to excite or invert C′, C^{α} and $C^{\alpha/\beta}$ spins, respectively, unless otherwise specified; the following pulse durations and shapes were used: 274 μs Q5 (and time reversed Q5) (Emsley and Bodenhausen, 1990) for π/2 C^{α}, C^{ali} pulses, 220 μs Q3 and 860 μs Q3 (Emsley and Bodenhausen, 1990) for π C^{ali} and C^{α} pulses, respectively, 500 μs Chirp shape (Boehlen and Bodenhausen, 1993) for adiabatic inversion of C′ and C^{α}.

The following 2D experiments were acquired: CACO-IPAP (Bermel et al., 2005) (with 1024×380 data points, 16–64 scans, depending on the sample), CBCACO-IPAP (Bermel et al.,

2005) (with 1024×380 data points, 32–64 scans, depending on the sample), CCCO-IPAP (Bermel et al., 2006a) (with 1024×256 data points, 32–96 scans, depending on the sample), CON-IPAP (Bermel et al., 2006a) (with 1024×256 data points, 32–64 scans, depending on the sample), CEN-IPAP (with 1024×1024 data points, 128 scans). The details of the latter experiment are reported in the supplementary material.

To remove the C′ signal splitting in the acquisition dimension due to the strong $J_{C'C^{\alpha}}$ coupling of 55 Hz, the IPAP approach was used. Thanks to the uniformity of the splitting-value, the insertion of an IP-AP filter at the end of the sequence permits to separate the in-phase and anti-phase signal components, that can be stored separately and linearly combined, after frequency shift of each of the two multiplet components to the center of the original doublet, to suppress the coupling (Nielsen et al., 1995; Bermel et al., 2005). Small variations in the $J_{C'C^{\alpha}}$ scalar coupling constant are not going to affect the chemical shift and, in any case, they are expected to be within the resolution of the experiment.

Spectra were processed using zero filling and linear prediction in the indirect dimension.

Proton resonances were calibrated with respect to the signal of 2,2-dimethylsilapentane-5-sulfonic acid (DSS). Nitrogen and carbon chemical shifts were referenced indirectly to the ^{1}H standard using a conversion factor derived from the ratio of NMR frequencies, as recommended for biomolecules (Markley et al., 1998).

The statistical analysis of secondary shifts was performed by using the program CSI (Wishart and Sykes, 1994) as well as with the program TALOS (Cornilescu et al., 1999).

Results and discussion

Thanks to the already available ^{1}H and ^{15}N chemical shift information (Arnesano et al., 2001b; Banci et al., 2001), a minimal set of NMR experiments out of the *protonless* NMR portfolio was sufficient to extend the assignment to the heteronuclei of the backbone (N, C′, C^{α}) and to C^{β} nuclei. In particular, we recorded a CON-IPAP experiment (Bermel et al., 2006a) on ^{13}C,^{15}N labeled apo-Atx1 and ^{13}C,^{15}N labeled apo-Ccc2. In contrast to the ^{1}H–^{15}N HSQC spectra, where some signals were absent (Arnesano et al., 2001b; Banci et al., 2001), all the expected signals are present in the CON-IPAP spectra (except for the first residue). Large part of the sequence-specific assignment available for both proteins from the proton-based experiments was immediately extended to the C′. In the few cases for which ^{15}N chemical shift information was ambiguous or absent, a CBC-ACO-IPAP experiment (Bermel et al., 2005) provided the residue-type information necessary to get a firm assignment of all the resonances. The latter experiment allows also extension of the assignment to C^{α} and C^{β} nuclei. The assignment of the backbone heteronuclei and of the C^{β} for apo-Atx1 and apo-Ccc2a is reported in the supplementary material (Tables SM1 and SM2) and are being deposited to BMRB.

The assignment of the heteronuclei of the backbone (N, C′, C^{α}) and of C^{β} nuclei constitutes a solid base to predict secondary structural elements (Wishart and Sykes, 1994) and dihedral angles (Cornilescu et al., 1999) of a protein. In the present case, the CSI program could predict the majority of the secondary structural elements identified in the solution structures of the proteins (Banci et al., 2001; Arnesano et al., 2001b), except for the last β strand (α-helices were found for residues 16–28 (α1) and 53–63 (α2) in Atx1 and 14–27 (α1) and 56–61 (α2) for Ccc2a as well as β-sheets for residues 6–11 (β1), 36–39 (β2), 44–51 (β3) in Atx1 and 2–9 (β1), 34–36 (β2), 41–47 (β3) in Ccc2a). For some of the residues in the metal binding site for which the amide proton was difficult to be detected and only a partial assignment was possible with the ^{15}N labeled sample (Ser 16, Gly 17 in Atx1, Ser 14 and Ala 15 in Ccc2a), the ^{13}C chemical shifts could be identified indicating that these residues are in the initial part of helix α1 in either protein. The heteronuclear chemical shifts of the two Cys in the MXCXXC metal binding loop are consistent with the presence of two reduced Cys and with the first one being next to a β strand and the second one being part of an α helix (Sharma and Rajarathnam, 2000) in agreement with the fact that the metal binding loop actually separates two definite elements of secondary structure (strand β1 and helix α1) present in these highly homologous proteins.

Heteronuclear mapping of complex formation for Atx1

To assess whether ^{13}C chemical shift variations are a sensitive probe for intermolecular interactions, we used CBCACO-IPAP and CON-IPAP experiments to monitor chemical shift changes when passing from the isolated proteins to the complex.

First, an equimolar amount of unlabeled Ccc2a was added stepwise to apo-Atx1. The heteronuclear resonances of Atx1 show no significant variations (the only chemical shift changes being smaller than 0.05 ppm for the C′ signals of residues 21, 25 and 62; data not shown), confirming that in the absence of Cu(I), protein–protein interaction does not occur (Banci et al., 2006). With the addition of 0.5 equivalents of Cu(I) some signals selectively shift, and the shifts increase with the amount of copper added. This is consistent with the formation of the Atx1–Cu–Ccc2a adduct in fast chemical exchange (on the NMR time scale) with the free species. In the CBCACO-IPAP and in the CON-IPAP spectra of the 1:1:1 adduct, the correlations of Thr 14 were missing, as well as the C'-C^{α} and the C'-$N_{(i+1)}$ correlation of Lys 62. These correlations reappear upon further addition of Cu(I). An overlay of a selected region of the CON-IPAP spectra of apo-Atx1 and of the adduct formed with one equivalent of Cu(I) and Ccc2a is shown as an inset in Figure 1, that reports the full CON-IPAP map recorded on apo-Atx1 and the corresponding signal assignment.

From the analysis of the ^{15}N and $^{13}C'$ chemical shift variations between apo-Atx1 and the complex, reported in panels A and B of Figure 2, it is immediately evident that chemical shift variations of carbonyl carbons are less scattered than those of nitrogen nuclei. The squared sum for the residuals displayed in Figure 2A, B are 66.7 vs. 5.0 for ^{15}N and $^{13}C'$, respectively. Even taking into account the spectral range of the corresponding resonances (about 12 ppm for $^{13}C'$ and 25 ppm for ^{15}N), these values clearly confirm that the variations in ^{15}N shifts are larger than those of $^{13}C'$. In panels C and D of Figure 2 the chemical shift differences observed upon complex formation for C^{α} and C^{β} nuclei are also reported. The region spanning residues 35–50 appears as the least affected by complex formation. Therefore the root mean square (m) within this part of the backbone is taken to evaluate the minimum significant chemical shift variation for each of the nuclei investigated. The values corresponding to $2m$, $4m$ and $10m$ were also set to define a small, a medium or a large variation in chemical shift. The complete set of chemical shift variations detected upon complex formation for backbone N, C′, C^{α} and for C^{β} are reported as Supplementary Material (in Table SM3 we have highlighted the values according to their magnitude in yellow, orange and red, respectively).

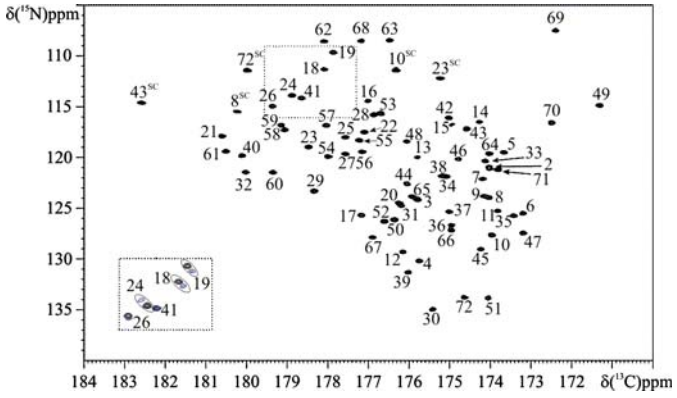

Figure 1. The CON-IPAP spectrum recorded on the ^{13}C,^{15}N labeled apo-Atx1 protein sample. All the expected backbone C'_i–N_{i+1} correlations, as well as the side-chain correlations expected for Asn (C^{γ}_i-N^{δ}_i) and Gln (C^{δ}_i-N^{ε}_i) residues are observed. The cross peaks are labeled according to the assignment; for the backbone C'_i–N_{i+1} correlations, the aminoacid number i is indicated. Side-chain correlations are further labeled with an 'SC' superscript to distinguish them from backbone ones. The inset shows the overlay of the CON-IPAP spectrum acquired on the same sample, after addition of one equivalent of Ccc2a (not shown as it is virtually identical to that of the apo-Atx1 protein alone) and after further addition of 1 equivalent of Cu(I) (gray). It can be clearly observed that several residues progressively shift upon Atx1–Cu(I)–Ccc2a complex formation (18, 19, 24) while others do not (26, 41).

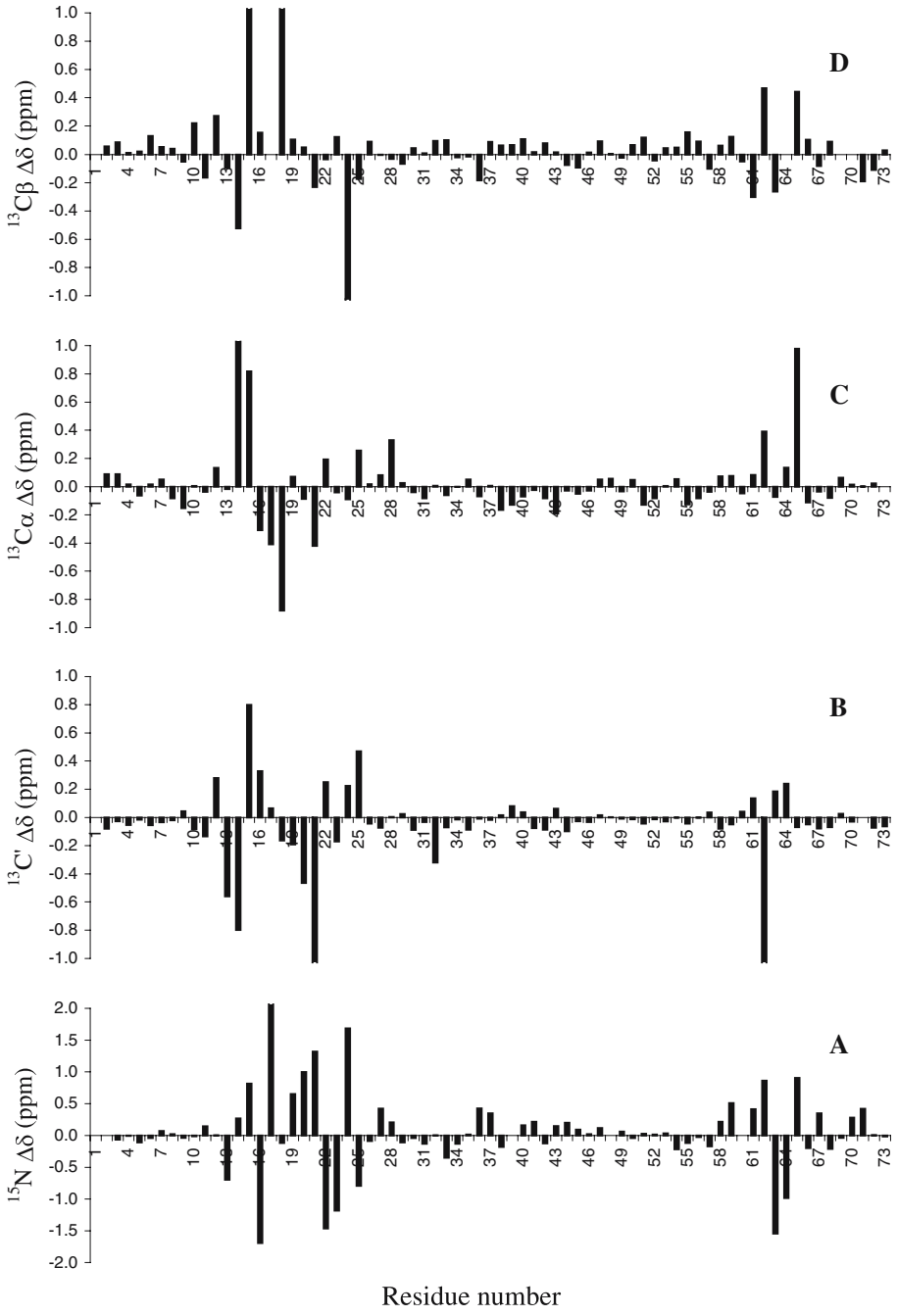

Figure 2. Variations of (A) N, (B) C′, (C) C^{α} and (D) C^{β} chemical shifts of Atx1 upon Atx1–Cu(I)–Ccc2a complex formation.

The analysis of the variations in ^{15}N chemical shift in the CON-IPAP maps permits a first identification of the interacting surfaces of Atx1 with Ccc2a. In particular, the N signals of Ser 16, Gly 17, Lys 24 and Thr 63 show remarkably high variations, but also Met 13, Cys 15, residues 19–24, Val 25, Lys 62, Gly 64, Lys 65 do show significant chemical shift variations. Furthermore, the ^{15}N chemical shifts of Thr 27, Ile 36, Lys 59, Lys 61, Val 67 and Lys 71 are affected by complex

formation. These data are consistent with those obtained with $^{1}H–^{15}N$ HSQC mapping (Arnesano et al., 2001a), even if in the latter spectra some signals (i.e. those of residues 1–4, 14, 16, 17, 22, 40) were not present either at the beginning or at the end of the titration, due to exchange with the solvent or conformational broadening of the H^{N} signals[1].

As far as carbon chemical shifts are concerned, the $^{13}C'$ signals of residues Met 13, Thr 14, Cys 15, Ala 21 and Lys 62 are showing the largest chemical shift variation upon complex formation; also Val 12, Ser 16, Gly 20, Val 25 and, to a lesser extent, the other residues in the stretch 11–24 and 61–64, show perturbed chemical shifts.

The relevance of this protein region is confirmed by the C^{α} data which exhibit the largest chemical shift variations for Thr 14, Cys 15, Cys 18 as well as Ser 16 and Gly 17. Also Lys 65 is significantly affected by complex formation.

For the C^{β}, Cys 15, Cys 18 and Lys 24 show the largest deviation, followed by other two Lys residues (62 and 65). These charged residues are considered most important for protein–protein recognition and stabilization of the complex. Therefore it appears that going from N to C′, C^{α} and finally to C^{β} the variations in chemical shift become somehow more selective, highlighting specific residues.

In the experimentally determined solution structure of the adduct, the surface of interaction between Atx1 and Ccc2a is very well defined (Banci et al., 2006). The intermolecular contacts mainly involve helix α1 of Atx1 with loop 5 of Ccc2a and the complementary helix α1 of Ccc2a with loop 5 of Atx1. Furthermore, contacts between loop 1 of Atx1 and helix α1 of Ccc2a as well as between the two α2 helices of each protein are clearly identified (see the central column of the Table SM3 of the Supplementary Material).

In Figure 4 the chemical shift variations obtained for all the nuclei investigated are mapped on the Atx1 (top) and Ccc2a (bottom) protein frames, respectively. On the panels on the extreme right the colored surfaces indicate those residues for which the variation in solvent exposure changes considerably upon complex formation to highlight the regions where intermolecular contacts occur. Helix α1 (16–28), the terminal part of helix α2 and loops 1 (12–15) and 5 (64–65) are indeed defining the regions where chemical shift variations are most marked in Atx1.

In the solution structure of the adduct the metal-binding site is relatively close to the surface, adjacent to the center of the region of intermolecular contact. Mutagenesis demonstrates that Cys 15 of Atx1 and Cys 13 of Ccc2a are essential for complex formation while Cys 18 of Atx1 and, to a lesser extent, Cys 16 of Ccc2a are not essential (Banci et al., 2006). In the structural model of the complex Cys 18 of Atx1 and Cys 16 of Ccc2 (the two *non-essential* cysteines) are buried in the complex interface, while Cys 15 of Atx1 and Cys 13 of Ccc2 remain solvent exposed with their side-chains protecting the metal binding site. Interestingly, the chemical shift variations observed in Atx1 are much more pronounced for Cys 15 than those observed for Cys 18. This is probably related to relatively larger conformational changes necessary for Cys 15 upon complex formation in order to transfer the copper ion and it is also consistent with the proposed role of structural support of Cys 18. Indeed, comparing the conformation of each of the two Cys residues in the apo form and in the complex, the two Cys have a different behavior. Cys 15, that in the apo form of the protein is not well defined and samples a large conformational space, adopts a specific conformation in the complex, that is different from the one when binding copper alone, consistent with its essential role in shuttling the copper ion upon complex formation. Cys18 is also quite disordered in the solution structure of the apo form; however the conformation that the backbone adopts upon Cu binding is maintained upon intermolecular, copper-mediated, complex formation. Some changes are observed for the side-chain. Consistently, the chemical shifts of backbone N and C′ do not show large variations upon complex formation, while C^{α} and C^{β} chemical shifts do. Interestingly, the chemical shift of Cys 15 carbon nuclei change more in the complex compared to the Cu-bound form, while the contrary holds for Cys 18.

The protein–protein contacts observed in the structure involve interactions between both hydrophobic and hydrophilic amino acids. Indeed, the protein–protein interaction surface is characterized by the presence of both charged and non-

[1]Of course, also the ^{15}N chemical shift values for Pro 31 and Pro 51 were missing in the previous analysis.

charged regions. Close to the metal-binding site, the inter-protein contacts mainly involve hydrophobic residues, while at the other edge of the interfacing area, contacts between complementarily charged side-chains are observed. The variation in chemical shifts of the heteronuclei matches the regions of interaction.

Heteronuclear mapping of complex formation for Ccc2a

A similar analysis was also accomplished for Ccc2a and the results are reported in Figure 3 and in the Supplementary Material (Table SM3), as well as in Figure 4 (bottom).

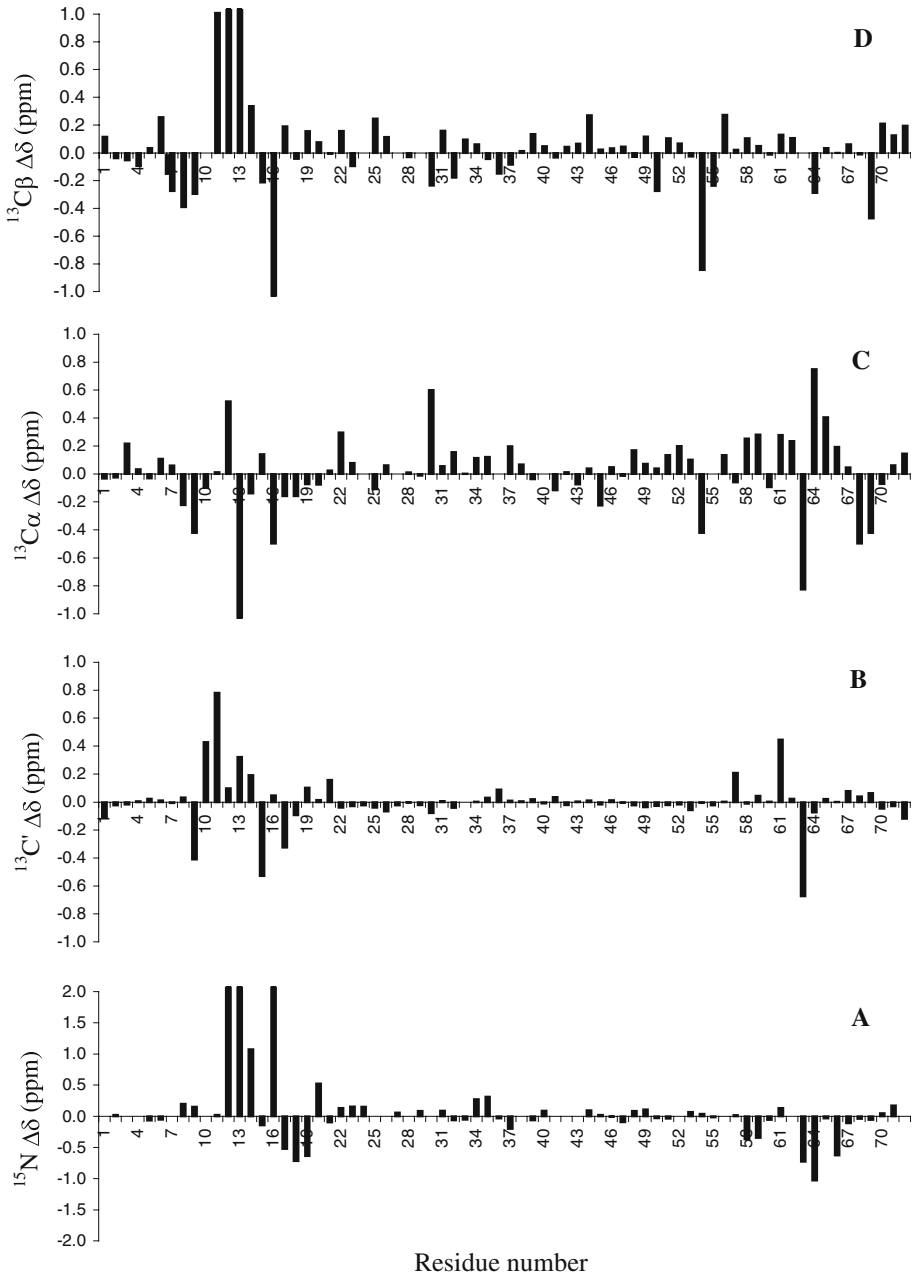

Figure 3. Variations of (A) N, (B) C′, (C) C^{α} and (D) C^{β} chemical shifts of Ccc2a upon Atx1–Cu(I)–Ccc2a complex formation.

The analysis of the variations in ^{15}N for Ccc2a shows the majority of the variations in the 12–20 and 58–66 regions. Indeed, the largest differences are observed for Thr 12, Cys 13 and Cys 16, followed by Ser 14, Asn 18 and Thr 19 and by Gly 63, Phe 64 and Cys 66. Also other neighboring residues are affected to a lesser extent. The data are consistent with those obtained with ^{1}H–^{15}N HSQC mapping (Arnesano et al., 2001a), clearly pointing out the region of the interaction with Atx1 that involves the two elements of secondary structure flanking the metal binding loop and the region 58–66.

As far as the $^{13}C'$ is concerned, the major variations are also clustered in the same region as observed for ^{15}N with a few additional residues in strand β1 also experiencing very large variations (His 9, Gly 10, Met 11), behavior similar to Atx1. Moreover, very large shifts are observed for Cys 13, Ala 15, Thr 17, Asp 61 and Gly 63. For the C^{α} data the largest chemical shift variations are again for Cys 13, Cys 16, Gly 63 and Phe 64 while for the C^{β} Met 11, Thr 12, Cys 13, Ala 15 and Leu 69 are most affected by complex formation.

Also in the case of Ccc2a the chemical shift variations nicely match the regions where the protein–protein contacts occur (mainly residues 11–16, 19, 23, and 60–64), and the combination of these data map the interaction surface.

As far as the metal binding Cys residues are concerned, the behavior is analogous to that observed for Atx1. Among the two Cys in the conserved metal binding MXCXXC motif, the first one (Cys 13), experiences large shifts for all the nuclei (N, C′, C^{α} and C^{β}), while the other (Cys 16), experiences smaller shift changes (except for the amide nitrogen). This is in agreement with the proposed role of support for Cys 16, more buried in the interaction surface, and an active role in shuttling the metal ion for Cys 13.

Other information on the complex

In the CON-IPAP and/or CBCACO-IPAP spectra the correlations involving the carbonyl/carboxyl moiety of Glu, Gln, Asp and Asn are also present. These can thus be analyzed in order to monitor chemical shift changes that occur to the side-chains upon Atx1–Cu(I)–Ccc2a complex formation.

For Atx1 the data show that only two side-chain nuclei have small but significant chemical

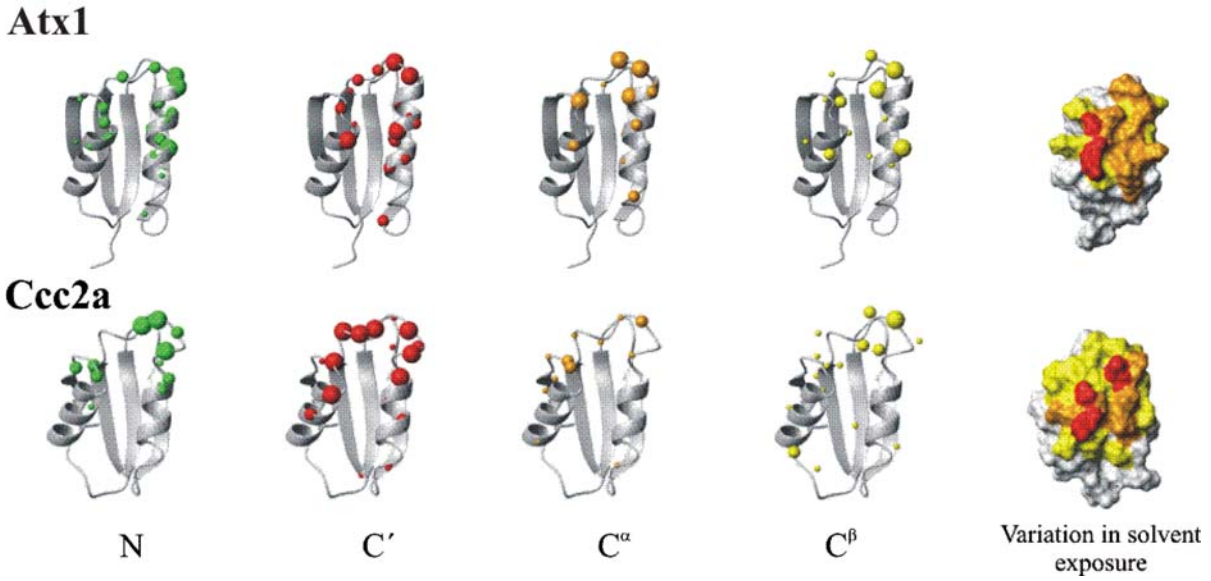

Figure 4. Mapping chemical shift variations upon Atx1–Cu(I)–Ccc2a complex formation on the protein structures of Atx1 and Ccc2a. For sake of clarity, variations of N, C′, C^{α} and C^{β} chemical shift are reported in four different panels as spheres (green for N, red for C′, orange for C^{α} and yellow for C^{β}). The radius of the spheres is correlated to the magnitude of the observed shift variations. Data for Atx1 are reported in the top row, while data for Ccc2a are reported in the bottom row. On the panels on the extreme right the surfaces of the two proteins (Atx1 on top, Ccc2 on the bottom) are color coded according to the extent of variation in solvent exposure upon complex formation (red corresponds to the maximal variations).

shift changes; these are the Asn 23 CO^{γ} and the Gln 43 CO^{δ}. The latter residue, as already established, forms an intramolecular H-bond with Met 13, stabilizing the binding loop conformation after copper uptake (Arnesano et al., 2001b). Asn 23, instead, is next to Lys 24, a residue necessary for complex formation.

For Ccc2a small variations were identified for the CO^{γ} of Asn 18 and 21 as well as for the CO^{δ} of Glu 57 and 60. Also the chemical shift of the $N^{\delta 2}$ of Asn 21 shows small but significant variation. Residues 18 and 21 belong to the interacting $\alpha 1$ helix, with Asn 18 facing the metal binding loop of Atx1. Glu 57 and 60 are found in the solution structure family of the adduct sometimes involved in electrostatic interactions with the complementary positively charged Lys residues of Atx1.

Atx1 has several lysine residues considered important for protein–protein recognition and interaction. To be able to detect selectively the side-chain terminal part of these residues we designed a novel CEN-IPAP experiment (see supplementary material for sequence details), that allowed us to detect the C^{δ}–N^{ε} Lys correlations and thus to monitor directly their chemical shift variations.

With the aid of a CCCO-IPAP experiment on apo-Atx1 and Atx1–Cu(I)–Ccc2a complex, the sequence-specific assignment was extended to the side-chains of these residues. In the CEN-IPAP spectrum of apo-Atx1, reported in Figure 5 (left), several resonances are readily observable. Most of the signals fall in the usual chemical shift range but one: the N^{ε} signal of Lys 65 falls 6 ppm downfield with respect to the expected range. It is possible

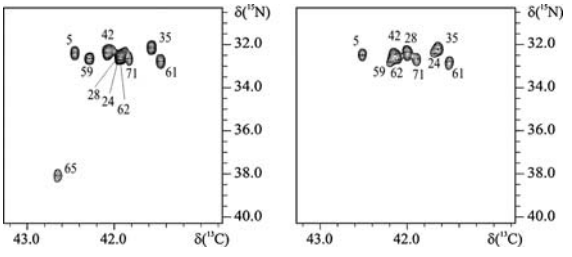

Figure 5. Comparison of the CEN-IPAP spectra for apo-Atx1 (left) and Atx1–Cu(I)–Ccc2a (right). The spectra were acquired with the pulse sequence and with the experimental parameters reported in the supplementary material. The cross peaks represent C^{δ}–N^{ε} Lys correlations and the labels indicate their sequence specific assignment.

that the terminal nitrogen is engaged in an H-bond interaction to prearrange the metal binding site for copper uptake.

The C^{δ} signals do not exhibit large variations. The spectral resolution in the direct dimension is high and allows us to measure small shifts. It can be observed that signals of Lys 5, 28, 31, 42, 61, and 72 do not show any shift, while 24, 59, 62, do shift more than 0.1 ppm. For Lys 65 the C^{δ}–N^{ε} correlation disappears and it is difficult to firmly establish if this is due either to conformational exchange processes that prevent observation of the signal or due to a shift in a crowded region. As Lys 65 is somehow buried in a hydrophobic patch at the interface, it may be important in stabilizing the hydrophobic core of the protein and the metal binding loop before metal binding and formation of the complex. In several conformers of the complex structure, intermolecular contacts are observed for the side-chain of Lys 65, which points towards a non-charged patch of the Ccc2a surface and seems involved in hydrogen bonds to the side-chain of Thr 19 or to the backbone of Cys 62. The chemical shifts of the nuclei of these Ccc2a residues are affected by complex formation.

It is somehow surprising that the chemical shift of the side-chain resonances of Lys 28 and 61 do not change significantly between the two species. However, according to the model of the adduct available, these two residues are at the edge of the interacting surface, and may be less relevant for complex formation.

Comparison of the 'protonless NMR' approach with the 'classical' approach

We would like to compare the results of the *protonless* approach with those previously obtained on the very same system using the standard approach based on ^{1}H–^{15}N HSQC mapping, also on the light of the available structural model (Banci et al., 2006). Indeed, the chemical shift mapping is widely used to identify interaction surfaces and it can be used to determine structural models of the interaction complex such as those obtained for the present complex using HADDOCK (Dominguez et al., 2003). Of course, chemical shift mapping is an indirect method to identify protein interaction surfaces since chemical shift changes may also occur as a result of secondary effects. In this frame, we want to assess here whether it is informative to

add information derived from experiments other than proton–nitrogen correlation experiments analyzing the results with the experimentally-determined structural model of the complex (Banci et al., 2006). Recent progress in calculations of chemical shifts, based on different methods (Wishart and Case, 2001; Neal et al., 2003) shows that different kinds of nuclei are affected to a different extent by all the possible interactions that can cause nuclear shielding in addition to the main random coil shifts typical of each nucleus (backbone and side-chain dihedral angles, ring current shifts, electric field effects, hydrogen bonds, solvent effects). Therefore monitoring variations of more than one type of nucleus can help having a more complete and robust picture of the interaction and to highlight the most relevant regions of the interacting proteins, eventually picking up additional structural features of the complex relevant for function.

The first evidence in comparing the results of the *protonless* NMR approach with the one previously obtained through the standard chemical shift mapping is that the heteronuclear data provide a more complete picture (Figure 6). Considering the *protonless* approach, that allows us to have information for four nuclei (N, C′, C^{α}, C^{β}), most of the residues could be mapped, while data for one of the forms were missing in ^{1}H–^{15}N HSQC experiments (residues 1–4, 14, 16, 17, 22, 40 for Atx1 and residues 1, 10, 12, 14, 15 for Ccc2a). It is true that appearance/disappearance of a signal upon a specific perturbation can be taken as evidence of the involvement of that residue in the occurring chemical process. However, direct monitoring of the residue is surely a more robust indicator and it may give some information on the magnitude of the effect. For example, the large ^{15}N shift observed for Gly 17 in Atx1 is indicative not only of the involvement of this residue in the interaction, but it can also give us some hints on the fact that the peptidic NH of this residue is probably undergoing changes in hydrogen bond interaction, as other minor perturbations are not sufficient to justify such a large chemical shift change. Indeed, large deshielding effect on amide ^{15}N nuclei (+5 to +8 ppm) has been observed upon hydrogen bonding (Case, 2000)

A surprising evidence is the small ^{15}N shift variation observed for Thr 14 and for Cys 18, since the two residues are part of the conserved

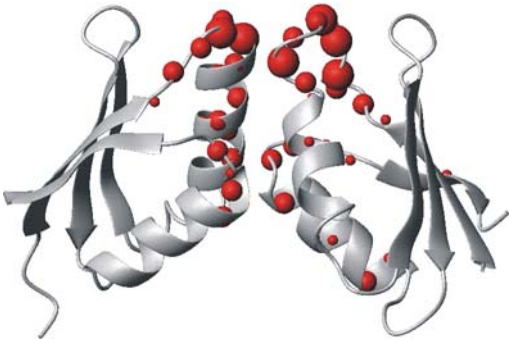

Figure 6. Chemical shift mapping of the backbone through *protonless* NMR experiments (CON-IPAP and CBCACO-IPAP). The data are mapped on the solution structure of the Atx1–Cu(I)–Ccc2a complex (Banci et al., 2006). The radius of the spheres is correlated to the magnitude of the 'combined' shift variations δ^{c} which, consistently with what proposed for ^{1}H–^{15}N HSQC mapping data (Grzesiek et al., 1996), are obtained when combining, for a specific residue, the chemical shift differences ($\Delta\delta_i$) for more than one type of nucleus according to $\delta^{c} = \sqrt{\frac{1}{n}\sum_{i=1}^{n}\left(\frac{\Delta\delta_i}{\eta_i}\right)^2}$, where $\Delta\delta_i$ is the chemical shift difference for the type of nucleus i (H^{N}, N, C′, C^{α} and C^{β}), η_i is the typical chemical shift range of nucleus i and n is the number of nuclei considered. The combined chemical shift obtained from *protonless* NMR experiments includes N, C′, C^{α} and C^{β}.

MXCXXC motif relevant for the chaperone function and the shifts observed for the other residues in this loop are very large. This could be an indication that more than one contribution to the nitrogen shift change upon interaction with different sign, summing up to a total effect that is actually negligible. Monitoring also carbonyl chemical shift variations gives an answer to this point, as the major variations observed actually involve residues 13–15.

The other large variations observed for carbonyls highlight the regions 12–25 and 62–64, consistently with the data obtained from nitrogen shift and actually expand the interacting region to include also the 12–14 region that was not clearly emerging from nitrogen perturbations. Carbonyl chemical shift variation of residue 32 is probably related to that of the nitrogen of residue 33 and, as both residues are quite far from the interaction surface, possibly due to induced structural changes.

Going to the C^{α} and C^{β} chemical shifts, the changes are on average smaller with large values at specific positions and in particular for the two cysteines (Cys 15 and Cys 18) that show large

variations in both the C^{α} and C^{β} shifts and for Thr 14 and Lys 65 (large C^{α} shift) and Lys 24 (large C^{β} shift). As pointed out above, the observed shifts for the two metal binding cysteines are in agreement with their different roles in shuttling the metal ion (Banci et al., 2006). The remaining large shifts observed highlight other key residues at the interface.

The other variations in chemical shifts observed for either C^{α} or C^{β} (or both) do match variations in solvent exposure upon binding of some residues, such as 16, 17, 21, 25, 28, 62–65 (see the right panels in Figure 5). The effect of solvent exposure on C^{α} and C^{β} chemical shifts has been nicely documented (Avbelj et al., 2004) and could account, at least partially, for the variations observed for C^{α} and C^{β} nuclei (16, 17, 21). The solvent effect is operative for C^{α} and C^{β} and is expected to influence also the other nuclei. The latter, however, are also largely affected by other effects and indeed display pronounced and uniform variations in the interaction region. Indeed, for example, residues 22 and 23, which lie in the part of the helix pointing towards the interior of the protein, do show nitrogen and carbonyl chemical shift changes, while the shift changes observed for C^{α} and C^{β} are actually small or negligible.

A similar overall picture is obtained when analyzing in detail the shifts observed for Ccc2a. Indeed the most pronounced chemical shift changes are observed for nitrogen, followed by C′, that allow us to additionally pick up some interesting regions (such as Gly 10, Met 11 and Ala 15), and complemented by C^{α} and C^{β} shifts that highlight key residues in the interaction (Met 11, Thr 12, Cys 13, Cys 16, Gly 63, Phe 64).

For all the nuclei investigated in the two proteins, some shift variations above the selected threshold are observed also for residues in regions of the protein far from the interaction site, such as in the residues 30–38 region. This may be the result of complexation-induced structural variations. Indeed, these residues belong to the β-sheet facing helix α1, the one most affected by complex formation.

Conclusions

Summarizing, the chemical shift changes of the different nuclei mapped through this *protonless* approach (N, C′, C^{α}, C^{β}) provide a robust description of the interaction surface upon formation of the Atx1–Cu(I)–Ccc2a complex. An advantage of the *protonless* approach consists of a more complete analysis of the protein. At the beginning of the titration, all the residues were observed through the CON-IPAP and CBCACO-IPAP experiments, while a few residues in the crucial metal-binding loop were not detected through the ^{1}H–^{15}N HSQC experiment due to solvent exchange processes affecting ^{1}H. The other important aspect that emerges from our study is that, even if all the data clearly indicate one specific interaction surface, and in this sense they agree one with the other, on the other hand each kind of nuclei that was mapped does display subtle difference with specific characteristics that can be related to the kind of nucleus investigated. As progress is being made in our understanding of which are the important factors that determine chemical shifts in proteins, it becomes clear that the different kinds of nuclei are affected to a different extent by the various interactions. This in turn means that chemical shift mapping using different types of nuclei will be able to pinpoint different effects occurring upon binding (variation in solvent exposure, in dihedral angles, in hydrogen bonding, etc). Therefore analysis of more than one kind of chemical shift can actually yield a different kind of information. In perspective, as our ability to reproduce through calculations the observed chemical shifts increases, it is possible to foresee that the chemical shift changes will be widely used to refine structural models.

The time required to acquire a CON-IPAP and a CBCACO-IPAP experiment is of course longer than that required to detect a ^{1}H–^{15}N HSQC experiment due to the intrinsic lower ^{13}C-sensitivity. However, with improvement of the hardware and with the use of cryo-cooled technology (Kovacs et al., 2005), the experimental time required to collect the pair CON-IPAP and CBCACO-IPAP is of the order of a few hours and it is foreseeable that it will be decreased even more in the near future. Therefore, we propose the use of the *protonless* experiments for chemical shift mapping of protein–protein interactions as an extra tool particularly important in difficult cases, such as interaction of unfolded proteins, which are nicely studied through the *protonless* approach (Bermel et al., 2006b), or to better characterize the

mobile or exchanging fragments, that are often those found in the interacting regions.

Acknowledgements

This work has been supported in part by the European Commission (QLG2-CT-2002–00988), and by the Italian MIUR. Dr. Alexandre Bonvin is gratefully acknowledged for the stimulating comments.

Supplementary material provided

The assignment of the heteronuclei in the backbone (N, C′, C^{α}) and of C^{β} of apo-Atx1 (Table SM1), of apo-Ccc2 (Table SM2), the chemical shift differences observed upon Atx1–Cu(I)–Ccc2a complex formation (Table SM3) and the CEN-IPAP pulse sequence (Figure SM1) are provided as Electronic Supplementary Material. It is available at http://dx.doi.org/10.1007/s10858-006-9068-z.

References

Arnesano, F., Banci, L., Bertini, I., Cantini, F., Ciofi-Baffoni, S., Huffman, D.L. and O'Halloran, T.V. (2001a) *J. Biol. Chem.*, **276**, 41365–41376.

Arnesano, F., Banci, L., Bertini, I., Huffman, D.L. and O'Halloran, T.V. (2001b) *Biochemistry*, **40**, 1528–1539.

Avbelj, F., Kocjan, D. and Baldwin, R.L. (2004) *Proc. Natl. Acad. Sci. USA*, **101**, 17394–17397.

Banci, L., Bertini, I., Ciofi-Baffoni, S., Huffman, D.L. and O'Halloran, T.V. (2001) *J. Biol. Chem.*, **276**, 8415–8426.

Banci, L., Bertini, I., Cantini, F., Felli, I.C., Gonnelli, L., Hadjiliadis, N., Pierattelli, R., Rosato, A. and Voulgaris, P. (2006) *Nat. Chem. Biol.*, **2**, 367–368.

Bermel, W., Bertini, I., Duma, L., Emsley, L., Felli, I.C., Pierattelli, R. and Vasos, P.R. (2005) *Angew. Chem. Int. Ed.*, **44**, 3089–3092.

Bermel, W., Bertini, I., Felli, I.C., Kümmerle, R. and Pierattelli, R. (2006a) *J. Magn. Reson.*, **178**, 56–64.

Bermel, W., Bertini, I., Felli, I.C., Lee, Y.-M., Luchinat, C. and Pierattelli, R. (2006b) *J. Am. Chem. Soc.*, **128**, 3918–3919.

Bertini, I., Duma, L., Felli, I.C., Fey, M., Luchinat, C., Pierattelli, R. and Vasos, P.R. (2004) *Angew. Chem. Int. Ed.*, **43**, 2257–2259.

Boehlen, J.-M. and Bodenhausen, G. (1993) *J. Magn. Reson. Ser. A*, **102**, 293–301.

Case, D.A. (2000) *Curr. Opin. Struct. Biol.*, **10**, 197–203.

Cornilescu, G., Delaglio, F. and Bax, A. (1999) *J. Biomol. NMR*, **13**, 289–302.

Dominguez, C., Boelens, R. and Bonvin, A.M.J.J. (2003) *J. Am. Chem. Soc.*, **125**, 1731–1737.

Emsley, L. and Bodenhausen, G. (1990) *Chem. Phys. Lett.*, **165**, 469–476.

Grzesiek, S., Bax, A., Clore, G.M., Gronenborn, A.M., Hu, J.-S., Kaufman, J., Palmer, I., Stahl, S. and Wingfield, P. (1996) *Nat. Struct. Biol.*, **3**, 340–345.

Huffman, D.L. and O'Halloran, T.V. (2000) *J. Biol. Chem.*, **275**, 18611–18614.

Kovacs, H., Moskau, D. and Spraul, M. (2005) *Prog. NMR Spectrosc.*, **46**, 131–155.

Markley, J.L., Bax, A., Arata, Y., Hilbers, C.W., Kaptein, R., Sykes, B.D., Wright, P.E. and Wüthrich, K. (1998) *J. Biomol. NMR*, **12**, 1–23.

Neal, S., Nip, A.M., Zhang, H. and Wishart, D.S. (2003) *J. Biomol. NMR*, **26**, 215–240.

Nielsen, N.C., Thøgersen, H. and Sørensen, O.W. (1995) *J. Am. Chem. Soc.*, **117**, 11365–11366.

O'Halloran, T.V. and Culotta, V.C. (2000) *J. Biol. Chem.*, **275**, 25057–25060.

Oldfield, E. (2002) *Annu. Rev. Phys. Chem.*, **53**, 349–378.

Pufahl, R.A., Singer, C.P., Peariso, K.L., Lin, S.-J., Schmidt, P.J., Fahrni, C.J., Cizewski Culotta, V., Penner-Hahn, J.E. and O'Halloran, T.V. (1997) *Science*, **278**, 853–856.

Rosenzweig, A.C. (2001) *Acc. Chem. Res.*, **34**, 119–128.

Schwarzinger, S., Kroon, G.J.A., Foss, T.R., Chung, J., Wright, P.E. and Dyson, H.J. (2001) *J. Am. Chem. Soc.*, **123**, 2970–2978.

Shaka, A.J., Keeler, J. and Freeman, R. (1983) *J. Magn. Reson.*, **53**, 313–340.

Shaka, A.J., Barker, P.B. and Freeman, R. (1985) *J. Magn. Reson.*, **64**, 547–552.

Sharma, D. and Rajarathnam, K. (2000) *J. Biomol. NMR*, **18**, 165–171.

Sitkoff, D. and Case, D.A. (1998) *Progr. NMR Spectrosc.*, **32**, 165–190.

Sun, H., Sanders, L.K. and Oldfield, E. (2002) *J. Am. Chem. Soc.*, **124**, 5486–5495.

Wishart, D.S. and Sykes, B.D. (1994) *J. Biomol. NMR*, **4**, 171–180.

Wishart, D.S. and Case, D.A. (2001) *Methods Enzymol.*, **338**, 3–34.

Zuiderweg, E.R. (2002) *Biochemistry*, **41**, 1–7.